Energy Storage Materials 61 (2023) 102839

Contents lists available at ScienceDirect

Energy Storage Materials

journal homepage: www.elsevier.com/locate/ensm

Electrohydrodynamically printed solid-state Photo-electro protein micro-capacitors

Nikita Paul [a], Lakshmi Suresh [a], Jaemin Seo [b], Yaoxin Zhang [a], Hangbo Zhao [b], Michael R. Jones [c], Swee Ching Tan [a,*]

[a] Department of Materials Science and Engineering, National University of Singapore, 9 Engineering Drive 1, Singapore 117575
[b] Department of Aerospace and Mechanical Engineering, University of Southern California, 3650 McClintock Avenue, Los Angeles, CA 90089, United States
[c] School of Biochemistry, Biomedical Sciences Building, University of Bristol, University Walk, Bristol, BS8 1TD, United Kingdom

ARTICLE INFO

Keywords:
Flexibility
Micro-capacitors
Electrohydrodynamic printing
Solid state
Indoor light
Photosynthetic protein

ABSTRACT

The rapid development of portable and scalable electronics requires the production of high-performing, miniaturized energy storage devices with great flexibility and dimensional liberty. In recent years, printed capacitors have emerged as a promising means of meeting these demands. Printed flexible solid-state capacitors are being considered as next-generation energy storage systems because of their flexibility, portability, low cost, scalability, long cycle stability and the option of charging or discharging securely. Here we use sustainable and toxin-free photosynthetic protein complexes to fabricate solid-state flexible Photo-electro micro-capacitors as flexible power packs that are operable under indoor illumination. Electrohydrodynamic (EHD) printing was used to print biohybrid Photo-electro protein micro-capacitors that exhibited high performance uniformity and operational stability. Devices could be connected in either series or parallel configurations to modulate the operating voltage window and charge-discharge time. A specific capacitance of 110 mF g^{-1} was obtained at a scan rate of 10 mV s^{-1} and was retained at 91% of the initial value after 10,000 charge/discharge cycles at a current density of 0.063 mA g^{-1}. Devices also displayed mechanical stability and robustness, retaining 93% of initial capacitance after 1000 cycles of bending. The data demonstrate that these micro-capacitors can deliver an economical and practical option as flexible energy storage and delivery devices for applications where exposure is primarily to indoor light.

1. Introduction

Energy storage devices such as capacitors, photocapacitors, fuel cells and batteries play key roles in a plethora of technological applications [1–3]. However, such devices are often bulky and/or heavy, and struggle to meet growing demands for power supplies that are lightweight, flexible and, increasingly, formed from renewable or biodegradable components. In recent years researchers have worked towards developing thin, flexible and compact energy storage systems that can meet the demand for technologies such as wearable electronics [4–7]. Flexible capacitors have been considered as a potential components of smart wearables due to their durability, cycle stability and sustained performance under continuous mechanical deformation [8–10]. However, the design of devices with flexibility and shape versatility continues to be a significant challenge. Currently, flexible capacitors are fabricated using methods such as spin coating [11], the use of sol gels [12,13], electrochemical deposition [14–16], chemical vapour deposition [17,18] and a range of printing procedures such as extrusion [19,20], fused deposition moudling [21,22] and injection [23–25]. Many of these techniques involve prohibitive costs, long production times, low efficiency and complex processing methods that hinder the large-scale development of flexible devices [26,27].

Among these approaches, printed capacitors can bring potential advantages such as patterning, better design diversity, tuneable size, compact architecture and excellent flexibility [28–30]. As examples, Lee et al. have used UV curing assisted stencil printing to developed a printed capacitor consisting of an SiO_2 nanoparticle-based electrolyte and activated carbon/multiwalled carbon nanotube electrodes. When printed on T-shirts the capacitor exhibited exceptional form factors, flexibility, and stability against laundering, wringing, ironing and folding [31]. Won et al. have fabricated an all-printed wearable, self-charging photocapacitor module made up of organic solar cells dubbed

* Corresponding author.
E-mail address: msetansc@nus.edu.sg (S.C. Tan).

https://doi.org/10.1016/j.ensm.2023.102839
Received 28 December 2022; Received in revised form 15 May 2023; Accepted 4 June 2023
Available online 5 June 2023

supercapacitors fibres. The woven photocapacitor module yield a voltage output of 3.2 V in ≈5 min under one Sun (100 mW cm^{-2}) illumination, achieving a final photo-conversion-and-storage efficiency of 4.94% at a discharge current of 3 mA. The cells demonstrated a high capacitance of ≈52 mF cm^{-2} with an energy density of 12.5 μWh cm^{-2}, and up to 96% retention of capacitance after 5000 charge/discharge cycles [32].

The main advantages of conventional capacitors and batteries are low production costs, long cycle life and the ability to be charged or discharged securely [33–35]. However, they typically use materials that are toxic and/or non sustainable [36–38], creating issues at end of life disposal. In addition, most energy storage devices use two different components for energy harvesting and energy storage. A progressive step in this area would be to explore the use of green, non-toxic and sustainable materials which can harvest, store and distribute energy in a single unit [39,40]. Candidate materials for this are natural pigment-protein biomacromolecules such as the "RC-LH1 complex" that enables solar energy conversion by purple photosynthetic bacteria [41]. This well-characterised system consists of a hollow cylindrical light harvesting (LH) domain that captures solar energy and transfers an excited electronic state to a central reaction centre (RC) which catalyses highly quantum-efficient photochemical charge separation [42]. The light harvesting "antenna" greatly enhances photon capture and energy conversion by the RC "transducer", enabling photosynthetic growth at the low light intensities found in the ecosystems these organisms inhabit. In a device setting the metastable charge separated state formed by the RC (a radical pair termed $P^{+}Q_{B}^{-}$)[43] can either initiate a photocurrent in a bio-photoelectrochemical cell or provide a means to store charge in a bio-photocapacitor (see Fig. 2**e**). Photosynthetic proteins are part of a broader range of natural materials that are of interest with respect to the provision of eco sustainable energy [43–45]. For example, Shen et al. recently demonstrated the very first example of a self-charging enzymatic supercapacitive biofuel cell to convert and store energy within a single device. The device possesses an operating regime (4.5 and 0.3 μW cm^{-2}, respectively) with an 80% residual activity after 50 charge/discharge pulses [46]. Khairy et al. have developed supercapacitors based on commercial 3D open-pore Ni foam and haem proteins. When tested at 0.4 mA discharge current, devices based on haemoglobin, myoglobin and cytochrome *c* generated specific capacitances of 13.8, 8.9 and 8.2 F g^{-1}, respectively [47].

A challenge in the design of biohybrid devices is the controlled deposition or patterning of the biomaterial on a supporting substrate or electrode surface, and one approach to addressing this is printing using a biomolecule ink. Of the printing technologies available commercially, electrohydrodynamic printing (EHD) is the least explored for the patterning of biomolecules [48,49]. Inkjet printing, screen printing and lithography are the most widely used technology in printed electronics. In Inkjet printing, ink is ejected from the nozzle by the pressure pulses generated from piezoelectric or thermal or pneumatic actuation. The protein ink used in this manuscript is sensitive to temperature; and high temperature leads to conformal disintegration of the protein molecules, making them no longer photoelectrochemically available/usable. Furthermore, inject printing requires specialized materials to be incorporated in the ink formulation to allow easy ejection of the ink. Another critical challenge of inject is its limited printing resolution, which is restricted to 20 μm. Reports have showed that EHD is capable of printing structures as low as 2 nm. Screen printing is also commonly used technique used for high resolution printing. However, it requires special requirements on the ink in order to transfer the pattern. It also requires a masque/stencil to fabricate the structures, which makes the printing process pretty time-consuming and expensive. Similarly, lithography also does not offer a general approach to high resolution, and it requires additional patterning systems and processing steps to define the printed structures. EHD priting technique exploits electrohydrodynamics to transfer ink from a nozzle to a substrate on a conducting X-Y stage by applying a voltage difference between the two [50–52]. In comparison to alternatives, the formation of protein micro-arrays by EHD printing has a number of advantages including being compatible with a large substrate area, inexpensive, rapid, versatile, and enabling formation of very precise micro and nanopatterns due to minimization of lateral variations in the droplet position as a consequence of distribution by the electric field [50,53]. The technique has been used to fabricate printed capacitors with a high specific capacitance and energy density. For example, Lee et al. successfully fabricated an ultra-high areal number density solid-state micro-capacitor directly on a chip using EHD printing that had an operating voltage of 65.9 V cm^{-2} [54]. Researchers have also used the technique to rapidly lay down highly uniform patterns of both single and multiple proteins over large areas [55]. Although researchers have attempted to print DNA micro arrays and patterns of proteins using EHD printing for cell cultures, there has been almost no attempt at using the technique to print photosynthetic proteins for functional applications like micro-photocapacitors. Deriving confidence from the current observation of charge storage ability with photosynthetic proteins, it can be attempted to design and print capacitors that can be used to power nano-micro- electronics.

In this work, we have used EHD printing to fabricate a solid state, flexible, biohybrid Photo-electro protein micro-capacitor (*MC*) that is operable under the low intensity lighting that is typically found in indoor settings. A micro-capacitor is a miniaturized, lightweight and portable passive circuit component that stores electrical energy in the form of electrostatic charges. It is widely used in microelectronics and usually consists of a thin film of dielectric material sandwiched between electrodes. The advantages of a solid-state system include ease of handling, scalability, increased safety and flexibility, high reliability, and tolerance of a wide range of operating temperatures [56–58]. The printed biohybrid *MC*s exhibited an optimal specific capacitance of 110 mF g^{-1} at a scan rate of 10 mV s^{-1} under only 0.002 Sun illumination, and showed excellent mechanical flexibility and operational stability. Cell voltage and charging-discharging time could be customised by simply connecting multiple devices in series or in parallel. Such printed solid-state devices show potential for the field of flexible, portable wearable electrochemical energy storage systems involving sustainable components.

2. Experimental

2.1. Materials

Non-conductive polyethylene terephthalate (PET) films were purchased from a LaTech Scientific Supply, Singapore. Platinum and tungsten inks were purchased from Sigma Aldrich. Distilled water (DI) was used for all experimental and cleaning purposes. RC-LH1 complexes lacking the PufX protein were purified as described previously using n-dodecyl β-D-maltopyranoside (DDM) as the isolating detergent [59,60]. They were stored as a concentrated solution in 20 mM Tris (pH 8.0)/0.04% (w/v) β-D-dodecyl maltoside (DDM) at −80 °C prior to use. Structural models of PufX-deficient RC–LH1 complexes are based on the X-ray crystal structure of the similar complex from *Thermochromatium tepidum* [61]. The concentration of RC-LH1 protein was such that the absorbence at 874 nm was equivalent to ~690 absorbence units cm^{-1}.

2.2. Photo-electro protein micro-capacitor fabrication and characterizations

Non-conductive PET films were washed thoroughly by sonicating continuously in ethanol for 30 mins, rinsed using DI water and dried. Square platinum and tungsten electrodes (0.9 cm^2) were printed at a separation of 1.5 cm using commercial platinum and tungsten inks. In this work, the working electrode (WE) is Platinum, which acts as a cathode and the counter electrode (CE) i.e., Tungsten is required to complete the electric circuit. The RC-LH1 protein solution was used for printing without further modification (**Supplementary Movie S1**). Inks

were housed in a syringe connected to an Enjet (Korea) EHD printing system (Fig. 1a). A voltage in the range 1 to 5 kV was applied to the nozzle attached to the syringe pump to generate an electrostatic field between the nozzle and the substrate, resulting in the formation of a meniscus at the nozzle tip due to the surface tension of the ink. When the electric field stress exceeded this surface tension the meniscus elongated in the direction of the field lines, resulting in the formation of an ink jet (Fig. 1b). Separation of nozzle and substrate was fixed at 50 μm and printing speeds were between 5 and 25 mm/s with multiple passes. Loadings of RC-LH1 complexes for 7, 14, 21 and 35 printing passes were calculated to be 32, 41, 46 and 60 mg cm^{-2}, respectively, based on changes in mass of the substrate. Devices were dried for 5 mins under ambient conditions after printing.

2.3. Device characterization

Printing of protein complexes and electrode materials was carried out using an EHD printer (Enjet, Korea) with a digitally controlled pressure pump. Cyclic voltammetry (CV), Electrochemical Impedance Spectroscopy (EIS) and Galvanostatic Charge/Discharge (GCD) measurements were carried out using a CHI 660 D electrochemical workstation under ambient laboratory light (0.002 sun). CV measurements

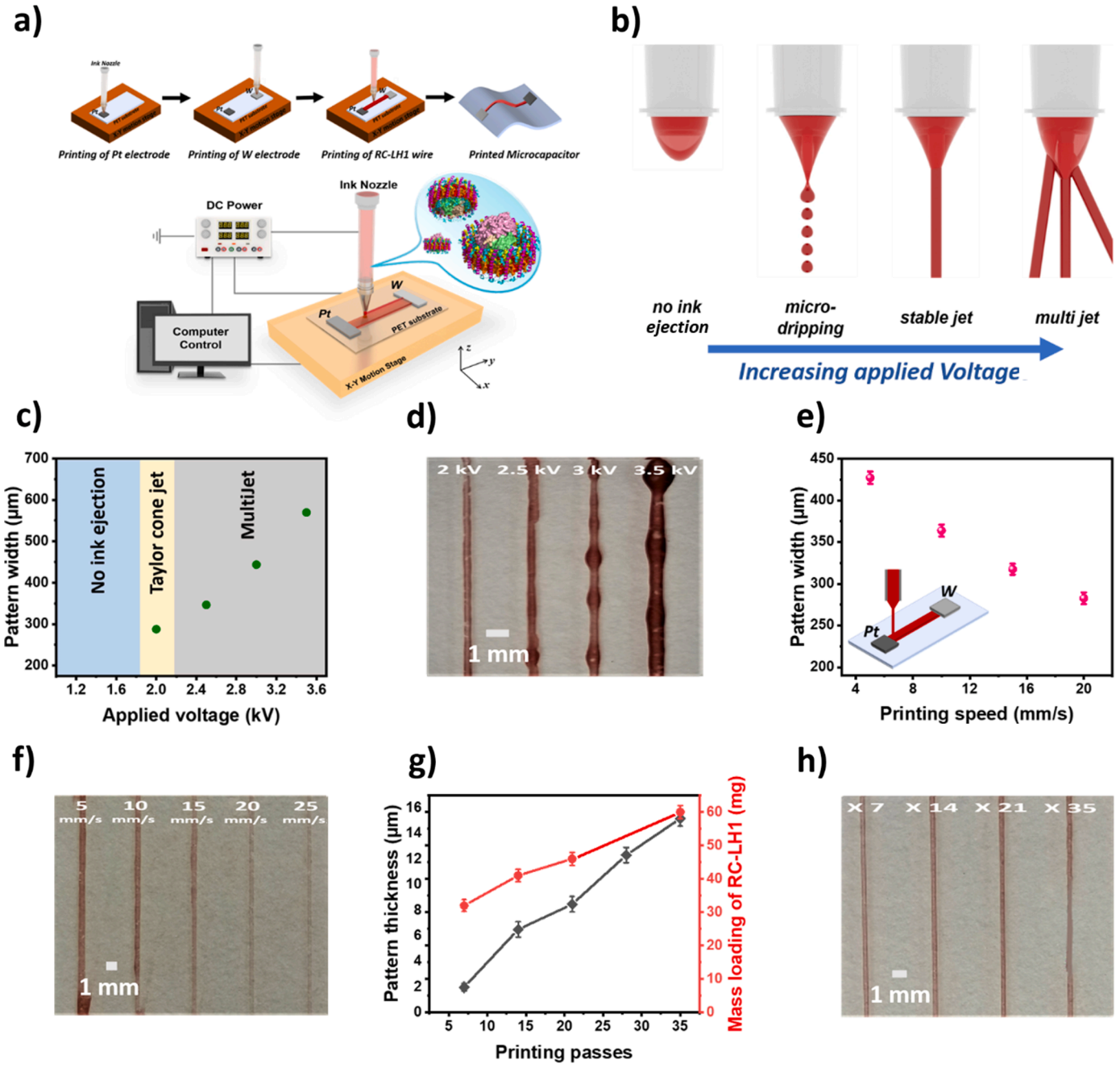

Fig. 1. Device fabrication. a) Schematic of the EHD printing of a biohybrid MC comprising a Pt electrode, W electrode and a connecting RC-LH1 protein line deposited from the ink nozzle onto a PET substrate on an X-Y stage. b) Schematic of ink behaviour as a function of applied voltage. c) Width of the printed protein line as a function of the voltage applied between the nozzle and the X-Y stage. d) Image of the RC-LH1 protein lines achieved at different applied voltages. e) Width of the printed protein line as a function of printing speed. f) Image of the RC-LH1 protein lines achieved at different printing speeds. g) Thickness (depth) of printed protein lines and mass loading of RC-LH1 proteins as a function of the number of printing passes. h) Image of the RC-LH1 protein lines achieved with different numbers of printing pass.

were conducted in a voltage range of 0–1 V with voltage sweep rates from 10 to 100 mV/s. EIS was recorded over a frequency range of 10^{-1} to 10^5 Hz at 0 V with an amplitude of 10 mV. GCD measurements were carried out at various current densities ranging from 0.013 to 0.08 mA cm^{-2}. Absorbence of the RC-LH1 protein solution was recorded using a Shimadzu UV–Vis spectrophotometer. Rheological tests were carried out using an Anton Paar modular compact rheometer (MCR302) with a parallel plate probe (PP25-SN 17002). Measurements were performed using 1 mL of sample in rotation mode. An Alpha Step D500 Profiler (KLA Tencor) was used to record the printed pattern thickness/height of the protein wire. The mechanical flexibility of the EHD-printed electrodes was quantitatively measured using a universal tensile machine (DA-01, Petrol LAB).

Specific capacitances (C, F/g) were calculated from the CV curves according to:

$$C = I\Delta V/(\upsilon mV),$$

where I is the current density (A/cm^2), ΔV is the voltage range, V is the potential (V), υ is the potential scan rate (mV/s), and m is the mass of the electroactive materials in the electrodes (g/cm^2) [64].

Areal capacitances were calculated using:

$$C_{areal} = I\Delta t/A\Delta V$$

where I is the current, Δt is the discharge time, A is the total area of the electrode, ΔV is the operating voltage window.

Volumetric capacitances were calculated using:

$$C_{volumetric} = I\Delta t/V\Delta V$$

where V is the total volume of the device.

3. Results and discussion

Biohybrid Photo-electro protein *MCs* were printed on a non-conductive PET film substrate. They consisted of a single line of deposited protein connecting printed square platinum and tungsten electrodes that were 1.5 cm apart (Fig. 1a). Scanning Electron Microscopy (SEM) image of the EHD printed RC-LH1 protein ink on PET substrate shows that the ink printing is in the form of cylindrical pattern **(Figure S1 in Supplementary Information)**. The protein ink was a concentrated solution of purified RC-LH1 complexes in 20 mM Tris buffer (pH 8.0)/0.04% DDM. This RC-LH1 ink showed shear thinning behaviour, the viscosity decreasing with an increase in shear rate (**Figure S2a in Supplementary Information**). As a consequence of the bacteriochlorophyll and carotenoid pigmentation of the RC-LH1 complexes (**Figure S2b in Supplementary Information**) the ink provided light harvesting capacity in the near-ultraviolet, in the blue and green regions of the visible spectrum, and in the near infrared [62]. For effective EHD printing with the RC-LH1 ink and the inks used to print electrodes, a series of parameters were optimized (**Table S1**). It was found that varying the strength of the applied voltage used to discharge ink from the nozzle tip led to different jetting modes (Fig. 1b). At low voltages there was no discharge due electrostatic forces being too weak to overcome the surface tension of the liquid, and on increasing the voltage some micro-dripping was seen in which gravity assisted some droplet discharge from the nozzle tip [53]. When the applied voltage reached 1.8 kV a thin thread of liquid (cone jet) was ejected that formed narrow and relatively uniform patterns (Fig. 1c, d). At voltages above 2.2 kV more complex and tilted jets were formed (multi jetting) leading to a larger print width and poor uniformity (Fig. 1c, d) [63]. It was thus concluded that the ideal DC voltage for the cone-jet mode was in the range of 1.8 to 2.2 kV. Line width was found to decrease with increased printing speed (Fig. 1e, f), and line height/density was found to increase with the number of printing passes, increasing the mass loading of RC-LH1 protein complexes while maintaining a constant line width (Fig. 1g, h). Conditions of 35 cycles at a printing speed of 25 mm/s produced optimal narrow uniform lines of ~280 μm width with a dense protein loading – these devices are referred to below as "standard *MCs*".

The electrical performance under simulated indoor lighting of printed *MCs* was explored by EIS and CV. Photocapacitance was demonstrated by comparing CV profiles in the dark and in the presence of 0.002 Sun illumination (Fig. 2a), and in the absence of a redox electrolyte to maximise capacitance (see **Figure S3 in Supplementary Information**). In the dark the devices showed a narrow CV curve indicative of non-capacitive behaviour. In contrast, illumination produced a pronounced vertical broadening of the curve indicating capacitive behaviour due to the photochemical activity of the RC-LH1 proteins. The specific capacitance, calculated as described in the Experimental section, was 64 mF/g under ambient light as compared to 7 mF/g in the dark. CV measurements at a scan rate of 100 mV/s over voltage windows between 0.1 and 1 V (Fig. 2b) produced CV curves that were always near rectangular in form, suggesting good capacitive behaviour, electrochemical stability and reversibility. A potential range of 1 V was chosen to investigate the cell's overall electrochemical activity in subsequent measurements as this produced the highest specific capacitance (**Figure S4 in Supplementary Information**). The shape of the curve obtained over a range of 1 V was maintained over a ten-fold variation in scan rate (Fig. 2c), again demonstrating good capacitive behaviour and a low resistance to electron transport within the device [65]. Since, the mass loading of the active materials was not high, areal and volumetric capacitances were also calculated, as described in the Experimental section. C_{areal} was 1.11 mF/cm^2 and $C_{volumetric}$ was 790 mF/cm^3.

EIS was used to investigate the effect of the width of the printed protein line on electrochemical performance. Protein lines of 283 μm, 318 μm and 427 μm in width were created by varying the printing speed. EIS data on the resulting *MCs* were fitted by a Randles equivalent circuit (**Figure S5 in Supplementary information**) consisting of an equivalent series resistance (R_s), a charge transfer resistance (R_{ct}), a Warburg resistance (Z_w) and a double-layer capacitance (C_{dl}). Nyquist plots showed a straight vertical line segment in the low-frequency region that is typical of capacitive behaviour (Fig. 2d). The inclined line in the medium-frequency region above the knee frequency corresponded to the Z_w. The equivalent series resistance (R_s) was the X-intercept in the high-frequency region (Fig. 2d), and the radius of the plotted semicircle plotted was representative of the R_{ct}. A gradual increase in R_s and R_{ct} with increasing protein line width (**Table S2**) indicated an increasingly unfavourable medium for ion diffusion, confirming the narrowest 280 μm width lines as being preferable.

The proposed mechanism of photoinduced charge storage is illustrated in Fig. 2e. Low intensity illumination produced photochemical charge separation inside the RCs creating electric dipoles throughout the protein array. As there is no electrolyte to efficiently transport these charges, oxidation at the tungsten anode and reduction at the platinum cathode results in the trapping of charge within the protein array, causing a potential across the device.

The influence of protein loading was examined by varying the number of EHD printing passes used to manufacture *MCs*. A broader CV curve was obtained for a device printed with 35 printing passes than devices formed from either 21, 14 or 7 passes (Fig. 3a) suggesting a dependence on the availability of RC LH1 complexes to perform charge separation. Analysis of these CV curves revealed a linear increase in specific capacitance with an increasing number of printing passes (Fig. 3b). In Nyquist plots of EIS data on these devices (Fig. 3c) the values of R_s and R_{ct} were inversely dependant on the number of passes (**Table S3**), lines formed from 35 passes having the highest values indicative of the worst electron diffusion kinetics. As indicated above, CV curves for the 35 pass device measured under indoor light (0.002 Sun) at three different scan rates between 10 and 100 mV/s were nearly rectangular in shape and symmetric, characteristics typical of conventional capacitors (Fig. 2c). In contrast, CV curves for devices formed with 7, 14 or 21 printing passes were non-rectangular and only partly

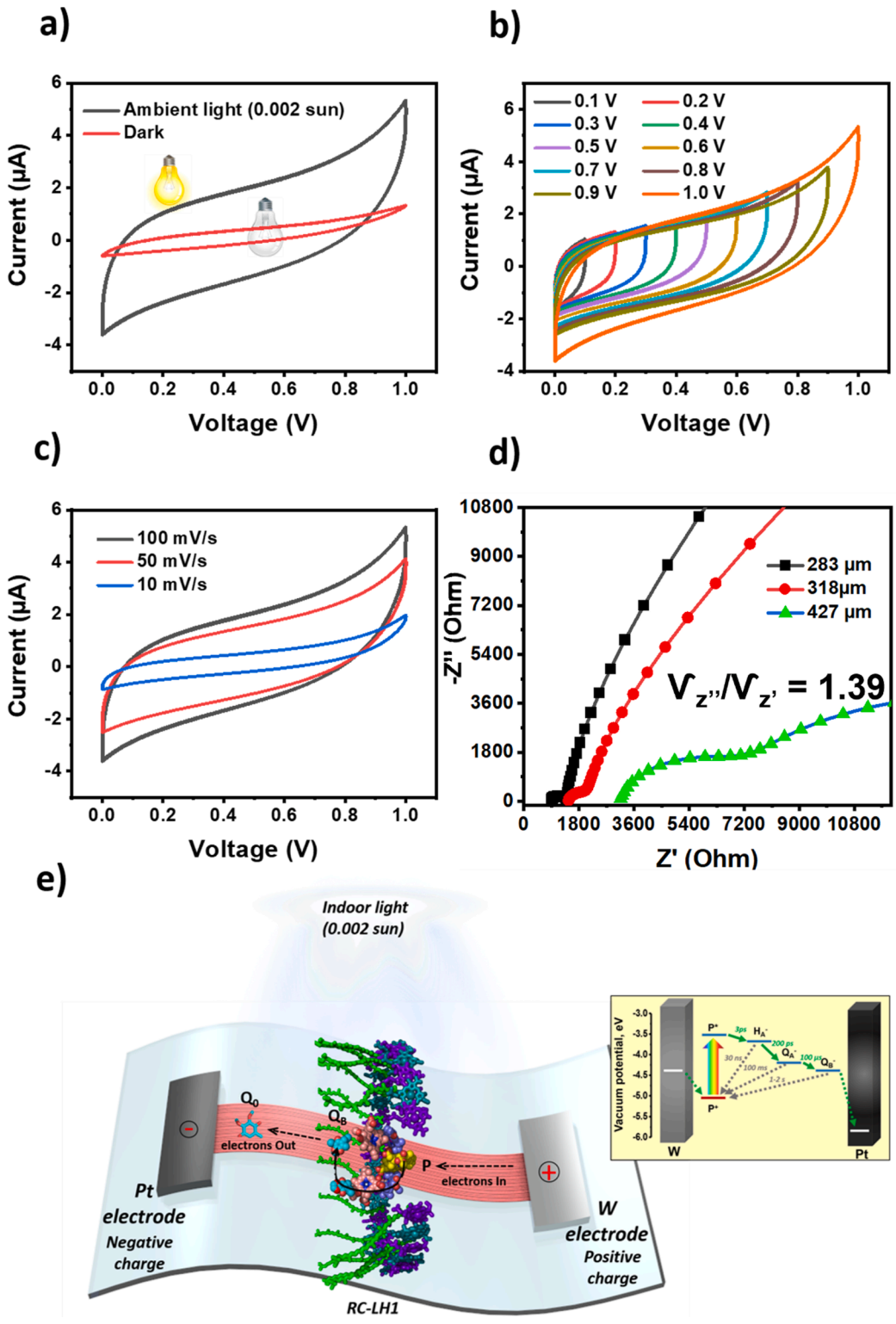

Fig. 2. Device characterisation. a) CV profiles (scan rate 100 mV/s) for a standard MC under indoor light (0.002 Sun) and in the dark. b) CV profiles (scan rate 100 mV/s) at different voltages for a standard MC under 0.002 Sun illumination. c) CV profiles at different scan rates for a standard MC under 0.002 Sun. d) Nyquist plots of EIS data for MCs with different protein line widths. e) Outline of the mechanism of charge separation and photocapacitance generated by RC-LH1 complexes. Photoexcitation triggers charge separation with the RC component between the primary electron donor bacteriochlorophylls (P) and the secondary acceptor ubiquinone (Q_B). Charge separation is initiated by photoexcitation of P into its first singlet excited state (P*), forming a P^+ cation at one "terminal" of the protein. Charge separation continues through the sequential formation of series of increasingly long-lived radical pairs ($P^+H_A^-$, $P^+Q_A^-$ and $P^+Q_B^-$). At each stage, rapid onward electron transfer (green solid lines) kinetically outcompetes slow recombination processes (grey dash lines) ensuring a high quantum efficiency. The electron is transferred across the protein to form an anion at the ubiquinone (Q_B^-) at the other "terminal" of the protein [43]. In the absence of any electrolyte, minimal electron transfer from the tungsten electrode or to the platinum electrode would be plausible, with the majority of the charges trapped within the protein multilayers giving rise to the device's capacitance.

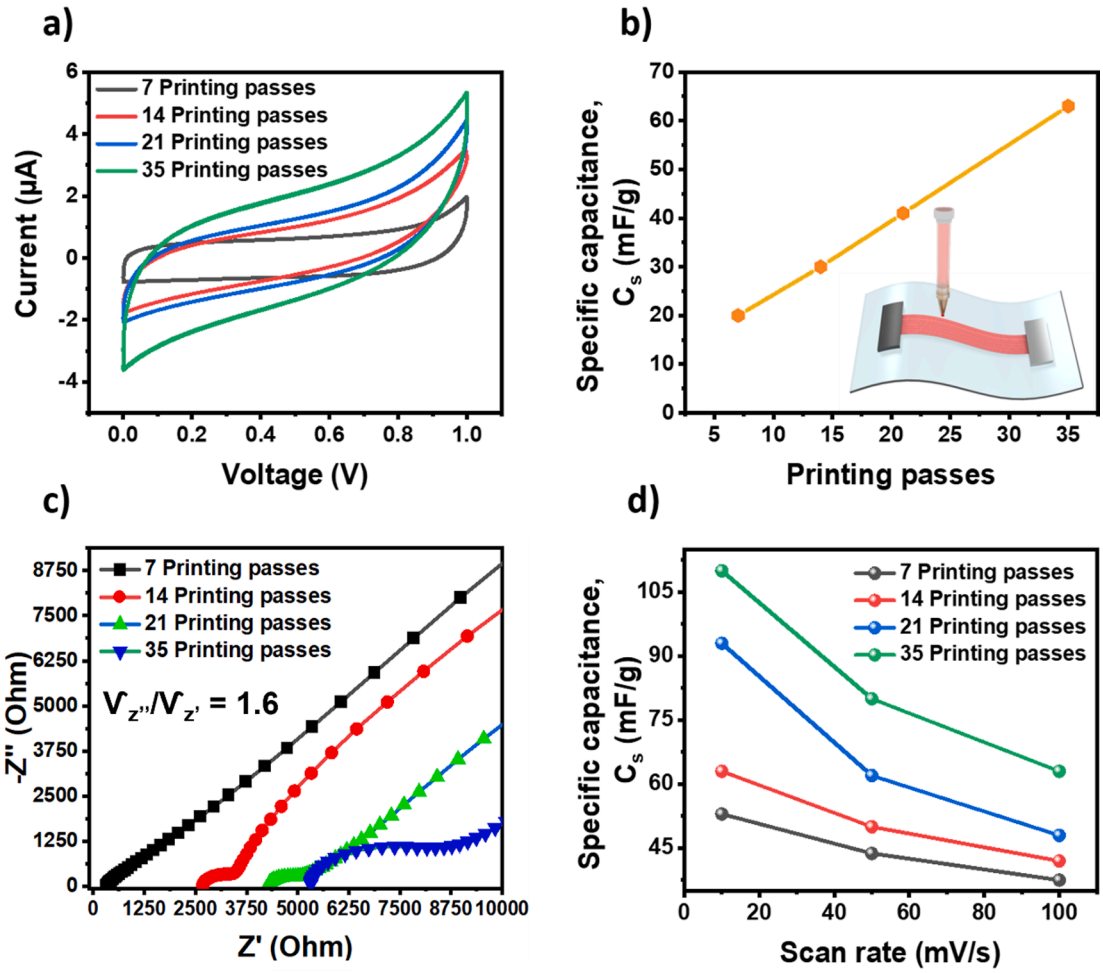

Fig. 3. Device optimisation. a) CV profiles (scan rate 100 mV/s) for MCs formed with different numbers of printing passes under 0.002 Sun illumination. b) Specific capacitances derived from the data in (a) for the four types of MC. c) Nyquist plots of EIS data for MCs formed with different numbers of printing passes. d) Specific capacitances derived from the data in (a) and **Figure S7a-c** for the four types of MC at three scan rates.

symmetric **(Figure S6 in Supplementary information)**, indicating less ideal behaviour. A single RC-LH1 complex has a maximum diameter of ~13 nm [40]. Hence, a printed pattern with 7, 14, 21 and 35 printing passes would contain ~150, ~500, ~650 and ~1170 stacked protein units respectively. Hence, more dipole units would be generated for the device with 35 printing passes compared to its counterparts. This in turn leads to higher dipole strength thereby affecting the overall cell capacitance. Variation of specific capacitance as a function of scan rate and number of printing passes is shown in Fig. 3d. The highest specific capacitance (110 mF g^{-1}) was for a 35 printing pass device at a scan rate of 10 mV s^{-1}. Despite the linearity displayed in Fig. 3b, printing involving more than 35 passes was not pursued as printing conditions became more difficult as the amount of protein loading increased due to air turbulence between nozzle tip and substrate surface, reducing the overall print quality and resolution [50].

Standard *MCs* displayed a symmetric galvanostatic charge-discharge (GCD) profile at current densities between 0.013 and 0.08 mA cm^{-2} (Fig. 4a), indicating excellent electrochemical reaction kinetics. Notably, the voltage drop as current flowed (IR drop) was also very small. For example, the GCD curve at 0.06 mA cm^{-2} showed an IR drop of only 0.052 V, indicating an excellent electrochemical performance [66,67]. Charge-discharge stability was examined for a standard *MC* at a constant current density of 0.06 mA cm^{-2}. Even after 10,000 cycles it demonstrated excellent electrochemical stability with 91% retention of its initial performance (Figure 4b; profiles for last six cycles are plotted in the inset). The energy/coulombic efficiency (η) of the *MC*, a parameter crucial for determining cycle stability [36], was determined from the ratio of discharging time (t_D) and charging time (t_C) when the charge–discharge current densities were equal, according to: $\eta = (t_D/t_C)$ *100% [36]. The average coulombic efficiency was found to be 96% for standard *MCs*. It has been previously discovered by Dr. Tan's lab, that charge transport in protein multilayers devoid of an electrolyte occurs through charge hopping between adjacent protein layers which is diffusion dependant thereby resulting in prolonged discharge times compared to electrolyte aided systems [40]. In the manuscript, direct evidence for charge storage capacity within RC-LH1 complexes/multilayers was demonstrated using Kelvin-probe and scanning-capacitance microscopy (KPFM). KPFM successfully suggested the charge trapping in a capacitor that not only harvests incoming light and segregates charges but also stores them. Power density (P), how quickly a capacitor can be charged, and energy density (E), how much energy can be stored [68], were determined from GCD curves at different current densities. A Ragone plot of energy density versus power density for a standard *MC* is plotted in Fig. 4b. The energy density and power density were calculated using formulae $E = 0.5$ CV [2] and $P =$ E/t, where t is the discharge time, respectively [68]. The standard *MC* displayed an energy density of between 5.0 and 4.1 mWh kg^{-1} over a power density range of 6.5 to 40 mW kg^{-1}

To explore the customisability of the device, three identical standard *MCs* were connected either in series or in parallel. Compared to a single *MC* (potential window: 1 V, discharge time: 50 s), the three *MCs* connected in series exhibited a three-fold increase in charge–discharge

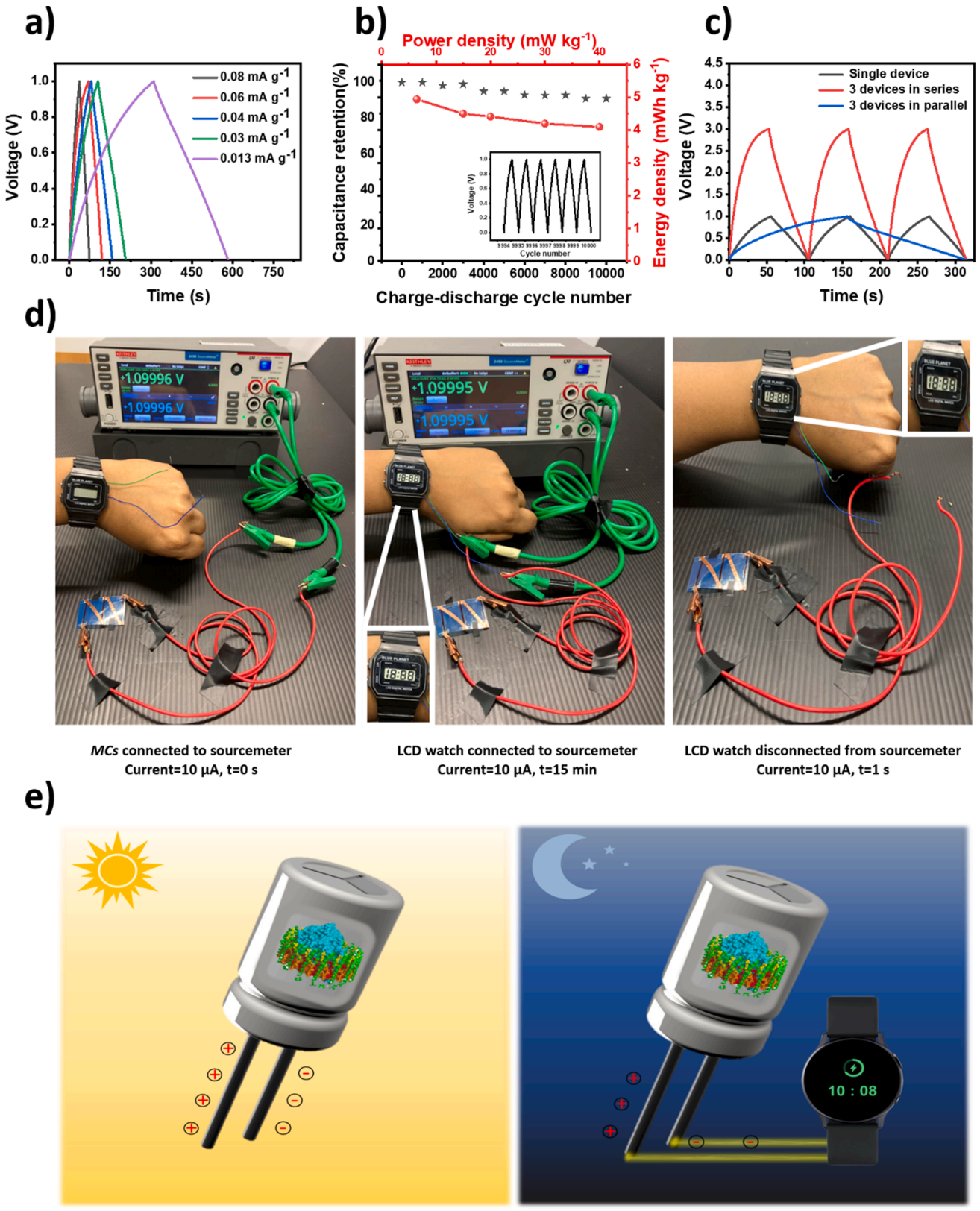

Fig. 4. Device performance and Storage of externally injected charges. a) GCD profiles for a standard MC at different current densities. b) Ragone plot for a standard MC and percentage retention of capacitance at a current density of 0.063 mA g^{-1} by a standard MC as a function of charge/discharge cycle number. Inset shows the GCD profiles for the last six charge/discharge cycles. c) Galvanostatic charge/discharge profiles collected at a current density of 0.063 mA g^{-1} for a single standard MC and for three connected in series or in parallel. d) Three MCs in series were connected to the sourcemeter (left image). LCD watch was connected to complete the circuit and external charges were injected for 15 mins by applying a constant current of 10µA (middle image). The sourcemeter was switched off and charged MCs powered an LCD watch for approximately 1–2 s (right image). Insets shows the zoomed in images of the LCD Digital watch. e) Schematic illustration demonstrating the standard MC based on bacterial light energy harvesting apparatuses.

voltage window (3 V) with almost the same discharge time (Fig. 4c, red) and the three *MCs* connected in parallel presented a three-fold increase in the discharge time (150 s) with 1 V voltage window (Fig. 4c, blue). This demonstrated simple manipulation of voltage and capacitance by merely designing the print pattern. Finally, three *MCs* were connected in series and were charged by applying a constant current of 10 μA for 15 mins. This provided sufficient charge to power up a low energy consumption LCD display watch for approximately 1–2 s (Fig. 4d, e).

Use of a PET film as the non-conducting substrate enabled the printing of a potentially flexible micro-capacitor (Fig. 5a). To evaluate feasibility, standard *MCs* were subjected to repeated deformation to a defined angle in a test rig (**Figure S7 in Supplementary Information**) and their electrochemical properties were tested. Bending to angles up to 180° had no significant effect on device CV profile (Fig. 5b) indicating preservation of structural integrity and the capacitive behaviour of the device. Calculated specific capacitance was unaffected except at the largest bending angle where a ~5% drop was seen (Fig. 5c). Similarly, GCD measurements also showed that bending had no significant effect on device performance (**Figure S8 in Supplementary Information**). This excellent stability extended over multiple deformations, with a 93% retention of specific capacitance obtained after 1000 bending cycles with a 135° bending angle (Fig. 5c).

4. Conclusions

In this work, we have demonstrated an all printed, solid state, flexible Photo-electro protein micro-capacitor that can utilize the low light intensities typically found in indoor settings. To achieve this, we have used as the photovoltaic component a natural photosynthetic protein that has evolved to convert low intensity solar energy with high quantum efficiency, having an architecture that surrounds the photovoltaic module (RC) with a highly quantum efficient solar energy collecting module (LH1). After optimisation, printed biohybrid micro-capacitors achieved a specific capacitance of 110 mF/g at a scan rate of 10 mV/s. The micro-capacitors had an output sufficient to power a nano/micro electronic device, delivering an energy density of 5 mWh kg^{-1} at a power density of 6.5 mW kg^{-1} and 4.1 mWh kg^{-1} at a power density of 40 mW kg^{-1}. The specific capacitance is proportional to photosynthetic efficiency; and are dependant on the wavelength of light absorbed by the protein complexes. The biggest disadvantage of photosynthetic protein-based devices is that their performance is limited by slow diffusion processes rather than the ability of proteins to absorb light energy and separate charge. The efficiencies are also restricted by the laws of thermodynamics i.e., there is a theoretical limit to the highest achievable efficiency. In real scenario, these photosynthetic bacteria don't use all incoming light (due to respiration, reflection, light inhibition and light saturation) which reduces the overall photosynthetic efficiency to be between 3%–6% based on total solar radiation. On top of this, the incident light intensity used in our work was only 0.002 Sun (indoor setting light), which further reduces the generation of photoactive charges. In this case, different approaches could be used to expand the output of these micro-capacitors, but there are practical limitations. We tried using higher concentrations of RC-LH1 to improve reaction flux and light harvesting but the solution was already highly concentrated and, by its nature, highly viscous and challenging to form a cone-jet ink. Also, depending on the configuration of a device, adding more protein by increasing thickness or concentration can produce diminishing returns due to self-shading, increased diffusion lengths and so on. So, increasing the concentration or thickness of patterns did not necessarily increase the capacitance and pose additional technical challenges. However, there is still lot of room to further optimize the performance of these micro-capacitors through design optimization. It has been found that several light trapping structures like metal nanoparticles, surface plasmons, photonic crystals, Johnson solid reflectors, light couplers have a great potential in the enhancement of the optical absorption and conversion efficiency across a wide wavelength range, as does the addition of synthetic and or natural accessory light harvesting pigments.

The EHD printed devices were operationally and mechanically robust retaining 91% of their initial capacitance after 10,000 charging/discharging cycles and 93% of their initial capacitance after 1000 bending cycles. We connected three micro-capacitor units in both series and parallel for efficient power source. The data demonstrate that such printed flexible micro-capacitor have a promising future as flexible energy-storage modules for robotics and wearable electronic devices. Additionally, the work provides new insights into the development of solid state Photo-electro micro-capacitors based on bio sustainable and environmentally benign photosynthetic proteins.

CRediT authorship contribution statement

Nikita Paul: Conceptualization, Methodology, Investigation, Data curation, Formal analysis, Writing – original draft, Writing – review & editing. **Lakshmi Suresh:** Conceptualization, Investigation, Data curation, Formal analysis. **Jaemin Seo:** Visualization, Data curation, Formal analysis. **Yaoxin Zhang:** Visualization. **Hangbo Zhao:** Data curation, Formal analysis, Investigation, Writing – review & editing. **Michael R. Jones:** Funding acquisition, Validation, Writing – review & editing. **Swee Ching Tan:** Conceptualization, Validation, Supervision, Funding acquisition, Project administration.

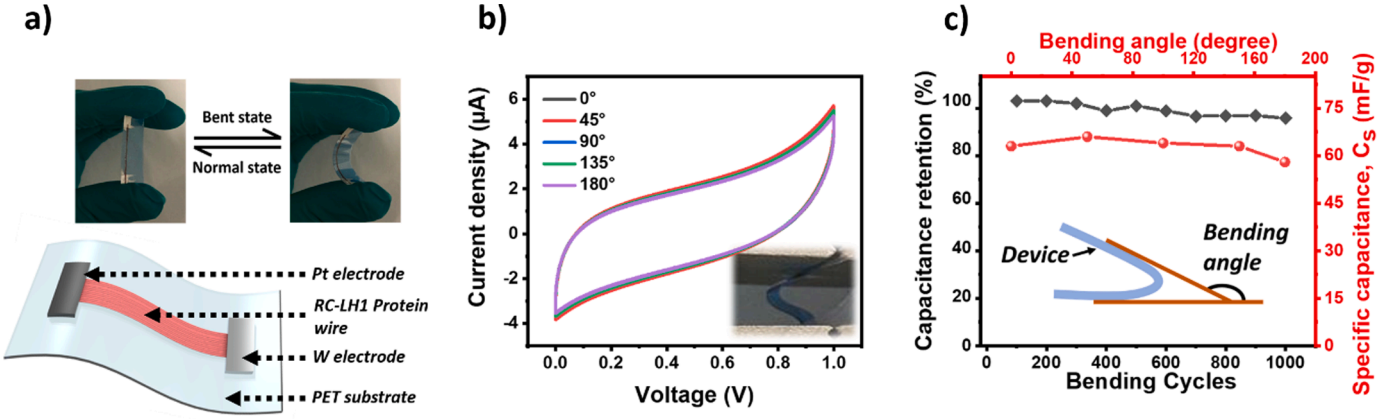

Fig. 5. Device mechanical and operational stability. a) Schematic illustrating the scale and flexibility a standard MC. b) CV profile (scan rate 100 mV/s) for a standard MC under different bending angles. c) Specific capacitance derived from the data in (a) as a function of bending angle (defined in inset) and variation in specific capacitance over 1000 bending cycles' for a standard MC, expressed as a percentage of initial capacitance.

Declaration of Competing Interest

The authors declare the following financial interests/personal relationships which may be considered as potential competing interests: Swee Ching Tan reports financial support was provided by MOE AcRF Tier 2 (A-0005415-01-00) of Singapore. Michael R. Jones reports financial support was provided by Biotechnology and Biological Sciences Research Council of the UK.

Data availability

Data will be made available on request.

Acknowledgments

S.C.T. acknowledges the financial support from MOE AcRF Tier 2 (A-0005415-01-00) of Singapore. M.R.J. acknowledges support from the Biotechnology and Biological Sciences Research Council of the UK (project BB/I022570/1).

Supplementary materials

Supplementary material associated with this article can be found, in the online version, at doi:10.1016/j.ensm.2023.102839.

References

[1] D.Y. Lee, et al., Unusual energy storage and charge retention in Co-based metal–organic-frameworks, Microporous Mesoporous Mater. 153 (2012) 163–165.
[2] S.H. Kazemi, F. Bahmani, H. Kazemi, M.A. Kiani, Binder-free electrodes of NiMoO4/graphene oxide nanosheets: synthesis, characterization and supercapacitive behavior, RSC Adv. 6 (2016) 111170–111181.
[3] H. Jiang, P.S. Lee, C. Li, 3D carbon based nanostructures for advanced supercapacitors, Energy Environ. Sci. 6 (2013) 41–53.
[4] J. Barber, B. Andersson, Too much of a good thing: light can be bad for photosynthesis, Trends Biochem. Sci. 17 (1992) 61–66.
[5] N.P. Hylton, et al., Loss mitigation in plasmonic solar cells: aluminium nanoparticles for broadband photocurrent enhancements in GaAs photodiodes, Sci. Rep. 3 (2013) 2874.
[6] Y.J. Kang, H. Chung, C.-H. Han, W. Kim, All-solid-state flexible supercapacitors based on papers coated with carbon nanotubes and ionic-liquid-based gel electrolytes, Nanotechnology 23 (2012) 65401.
[7] M.F. El-Kady, V. Strong, S. Dubin, R.B. Kaner, Laser scribing of high-performance and flexible graphene-based electrochemical capacitors, Science 335 (2012) 1326–1330.
[8] C. Duan, et al., Highly durable, coking and sulfur tolerant, fuel-flexible protonic ceramic fuel cells, Nature 557 (2018) 217–222.
[9] D.W. Kim, S.M. Jung, H.Y. Jung, A super-thermostable, flexible supercapacitor for ultralight and high performance devices, J. Mater. Chem. A 8 (2020) 532–542.
[10] L. Kong, C. Tang, H.-J. Peng, J.-Q. Huang, Q. Zhang, Advanced energy materials for flexible batteries in energy storage: a review, SmartMat 1 (2020).
[11] Z.-S. Wu, K. Parvez, X. Feng, K. Müllen, Graphene-based in-plane micro-supercapacitors with high power and energy densities, Nat. Commun. 4 (2013) 2487.
[12] S.-C. Pang, M.A. Anderson, T.W. Chapman, Novel electrode materials for thin-film ultracapacitors: comparison of electrochemical properties of sol-gel-derived and electrodeposited manganese dioxide, J. Electrochem. Soc. 147 (2000) 444.
[13] R. RN, R. RG, Sol-gel MnO2 as an electrode material for electrochemical capacitors, J. Power Sources 124 (2003) 330–337.
[14] N.H.N. Azman, H.N. Lim, Y. Sulaiman, Influence of concentration and electrodeposition time on the electrochemical supercapacitor performance of poly (3,4-ethylenedioxythiophene)/graphene oxide hybrid material, J. Nanomater. 2016 (2016), 5935402.
[15] C.M. Parnell, et al., Simultaneous electrochemical deposition of cobalt complex and poly(pyrrole) thin films for supercapacitor electrodes, Sci. Rep. 9 (2019) 5650.
[16] Y. Liu, et al., Supercapacitor with high cycling stability through electrochemical deposition of metal–organic frameworks/polypyrrole positive electrode, Dalt. Trans. 47 (2018) 13472–13478.
[17] J.J. Yoo, et al., Ultrathin planar graphene supercapacitors, Nano Lett. 11 (2011) 1423–1427.
[18] J.R. Miller, R.A. Outlaw, B.C. Holloway, Graphene double-layer capacitor with ac line-filtering performance, Science (80-.) 329 (2010) 1637–1639.
[19] T. Nathan-Walleser, et al., 3D micro-extrusion of graphene-based active electrodes: towards high-rate AC line filtering performance electrochemical capacitors, Adv. Funct. Mater. 24 (2014) 4706–4716.
[20] C. Zhu, et al., Supercapacitors based on three-dimensional hierarchical graphene aerogels with periodic macropores, Nano Lett. 16 (2016) 3448–3456.
[21] A. Tanwilaisiri, et al., Design and fabrication of modular supercapacitors using 3D printing, J. Energy Storage 16 (2018) 1–7.
[22] A. Tanwilaisiri, R. Zhang, Y. Xu, D. Harrison, J. Fyson, A manufacturing process for an energy storage device using 3D printing, in: 2016 IEEE International Conference on Industrial Technology (ICIT), 2016, pp. 888–891, https://doi.org/10.1109/ICIT.2016.7474869.
[23] L.T. Le, M.H. Ervin, H. Qiu, B.E. Fuchs, W.Y Lee, Graphene supercapacitor electrodes fabricated by inkjet printing and thermal reduction of graphene oxide, Electrochem. Commun. 13 (2011) 355–358.
[24] B. Li, et al., Direct inkjet printing of aqueous inks to flexible all-solid-state graphene hybrid micro-supercapacitors, ACS Appl. Mater. Interfaces 11 (2019) 46044–46053.
[25] A. Sajedi-Moghaddam, E. Rahmanian, N. Naseri, Inkjet-printing technology for supercapacitor application: current state and perspectives, ACS Appl. Mater. Interfaces 12 (2020) 34487–34504.
[26] T. Pandirengan, A. Marikani, M. Durairajan, Improvement in dielectric properties of CaCu3Ti4O12 thin film over Pt(111)/Ti/SiO2/Si substrate by spin coating method, Proc. Natl. Acad. Sci. India Sect. A Phys. Sci. Accepetd (2018).
[27] Aegerter, M. & Mennig, M. Sol-Gel technologies for glass producers and users. (2004). doi:10.1007/978-0-387-88953-5.
[28] G. Lee, et al., Fully biodegradable microsupercapacitor for power storage in transient electronics, Adv. Energy Mater. 7 (2017), 1700157.
[29] P. Giannakou, M.O. Tas, B. Le Borgne, M. Shkunov, Water-transferred, inkjet-printed supercapacitors toward conformal and epidermal energy storage, ACS Appl. Mater. Interfaces 12 (2020) 8456–8465.
[30] L. Liu, et al., Structure-designed fabrication of all-printed flexible in-plane solid-state supercapacitors for wearable electronics, J. Power Sources 425 (2019) 195–203.
[31] J. Liang, B. Tian, S. Li, C. Jiang, W. Wu, All-printed MnHCF-MnOx-based high-performance flexible supercapacitors, Adv. Energy Mater. 10 (2020), 2000022.
[32] W.-Y. Jin, M.M. Ovhal, H.B. Lee, B. Tyagi, J.-W Kang, Scalable, all-printed photocapacitor fibers and modules based on metal-embedded flexible transparent conductive electrodes for self-charging wearable applications, Adv. Energy Mater. 11 (2021), 2003509.
[33] S. Lee, et al., Integration of transparent supercapacitors and electrodes using nanostructured metallic glass films for wirelessly rechargeable, skin heat patches, Nano Lett. 20 (2020) 4872–4881.
[34] X. Peng, L. Peng, C. Wu, Y Xie, Two dimensional nanomaterials for flexible supercapacitors, Chem. Soc. Rev. 43 (2014) 3303–3323.
[35] X. Lu, et al., Stabilized TiN nanowire arrays for high-performance and flexible supercapacitors, Nano Lett. 12 (2012) 5376–5381.
[36] M. Rajkumar, C.-T. Hsu, T.-H. Wu, M.-G. Chen, C.-C Hu, Advanced materials for aqueous supercapacitors in the asymmetric design, Prog. Nat. Sci. Mater. Int. 25 (2015) 527–544.
[37] A. Railanmaa, S. Lehtimäki, J. Keskinen, D Lupo, Non-toxic printed supercapacitors operating in sub-zero conditions, Sci. Rep. 9 (2019) 14059.
[38] S. Huang, X. Zhu, S. Sarkar, Y Zhao, Challenges and opportunities for supercapacitors, APL Mater. 7 (2019), 100901.
[39] S.K. Ravi, et al., Bio-photocapacitive tactile sensors as a touch-to-audio braille reader and solar capacitor, Mater. Horizons 7 (2020) 866–876.
[40] S.K. Ravi, et al., Photosynthetic apparatus of Rhodobacter sphaeroides exhibits prolonged charge storage, Nat. Commun. 10 (2019) 902.
[41] R.J. Pugh, P. McGlynn, M.R. Jones, C.N. Hunter, The LH1–RC core complex of Rhodobacter sphaeroides: interaction between components, time-dependent assembly, and topology of the PufX protein, Biochim. Biophys. Acta - Bioenerg. 1366 (1998) 301–316.
[42] D.A. Semchonok, J.-P. Chauvin, R.N. Frese, C. Jungas, E.J. Boekema, Structure of the dimeric RC-LH1-PufX complex from Rhodobaca bogoriensis investigated by electron microscopy, Philos. Trans. R. Soc. Lond. B. Biol. Sci. 367 (2012) 3412–3419.
[43] S.K. Ravi, et al., A mechanoresponsive phase-changing electrolyte enables fabrication of high-output solid-state photobioelectrochemical devices from pigment-protein multilayers, Adv. Mater. 30 (2018), 1704073.
[44] M. Khairy, S.A. El-Safty, Hemoproteins-nickel foam hybrids as effective supercapacitors, Chem. Commun. (Camb). 50 (2014) 1356–1358.
[45] R.K. Pal, S.C. Kundu, V.K. Yadavalli, Fabrication of flexible, fully organic, degradable energy storage devices using silk proteins, ACS Appl. Mater. Interfaces 10 (2018) 9620–9628.
[46] F. Shen, et al., Supercapacitor/biofuel cell hybrid device employing biomolecules for energy conversion and charge storage, Bioelectrochemistry 128 (2019) 94–99.
[47] M. Khairy, S.A. El-Safty, Promising supercapacitor electrodes based immobilization of proteins onto macroporous Ni foam materials, J. Energy Chem. 24 (2015) 31–38.
[48] K. Barton, et al., A desktop electrohydrodynamic jet printing system, Mechatronics 20 (2010) 611–616.
[49] B. Zhang, et al., Electrohydrodynamic 3D printing of orderly carbon/nickel composite network as supercapacitor electrodes, J. Mater. Sci. Technol. 82 (2021) 135–143.
[50] J.-U. Park, et al., High-resolution electrohydrodynamic jet printing, Nat. Mater. 6 (2007) 782–789.
[51] Y. Han, J. Dong, Design of integrated ring extractor for high resolution electrohydrodynamic (EHD) 3D printing, Procedia Manuf. 5 (2016) 1031–1042.
[52] H.K. Choi, et al., Scaling laws for jet pulsations associated with high-resolution electrohydrodynamic printing, Appl. Phys. Lett. 92 (2008), 123109.

[53] M.S. Onses, E. Sutanto, P.M. Ferreira, A.G. Alleyne, J.A. Rogers, Mechanisms, capabilities, and applications of high-resolution electrohydrodynamic jet printing, Small 11 (2015) 4237–4266.
[54] K.-H. Lee, et al., Ultrahigh areal number density solid-state on-chip microsupercapacitors via electrohydrodynamic jet printing, Sci. Adv. 6 (2020) eaaz1692.
[55] K. Shigeta, et al., Functional protein microarrays by electrohydrodynamic jet printing, Anal. Chem. 84 (2012) 10012–10018.
[56] C. Huang, J. Zhang, N.P. Young, H.J. Snaith, P.S Grant, Solid-state supercapacitors with rationally designed heterogeneous electrodes fabricated by large area spray processing for wearable energy storage applications, Sci. Rep. 6 (2016) 25684.
[57] P. Yang, W. Mai, Flexible solid-state electrochemical supercapacitors, Nano Energy 8 (2014) 274–290.
[58] S. Zheng, et al., All-solid-state flexible planar lithium ion micro-capacitors, Energy Environ. Sci. 11 (2018) 2001–2009.
[59] V.M. Friebe, et al., Plasmon-enhanced photocurrent of photosynthetic pigment proteins on nanoporous silver, Adv. Funct. Mater. 26 (2016) 285–292.
[60] S.K. Ravi, et al., Enhanced output from biohybrid photoelectrochemical transparent tandem cells integrating photosynthetic proteins genetically modified for expanded solar energy harvesting, Adv. Energy Mater. 7 (2017), 1601821.
[61] S. Niwa, et al., Structure of the LH1–RC complex from Thermochromatium tepidum at 3.0 Å, Nature 508 (2014) 228.
[62] V.K. Singh, et al., Biohybrid photoprotein-semiconductor cells with deep-lying redox shuttles achieve a 0.7 V photovoltage, Adv. Funct. Mater. 28 (2018), 1703689.
[63] B. Zhang, J. He, X. Li, F. Xu, D Li, Micro/nanoscale electrohydrodynamic printing: from 2D to 3D, Nanoscale 8 (2016) 15376–15388.
[64] J. Yan, et al., Advanced asymmetric supercapacitors based on Ni(OH)2/Graphene and porous graphene electrodes with high energy density, Adv. Funct. Mater. 22 (2012) 2632–2641.
[65] Z. Weng, et al., Graphene–cellulose paper flexible supercapacitors, Adv. Energy Mater. 1 (2011) 917–922.
[66] M. Beidaghi, W. Chen, C. Wang, Electrochemically activated carbon micro-electrode arrays for electrochemical micro-capacitors, J. Power Sources 196 (2011) 2403–2409.
[67] M.Z. Esfahani, M. Khosravi, Stamp-assisted flexible graphene-based micro-supercapacitors, J. Power Sources 462 (2020), 228166.
[68] Z. Fan, et al., Asymmetric supercapacitors based on graphene/MnO2 and activated carbon nanofiber electrodes with high power and energy density, Adv. Funct. Mater. 21 (2011) 2366–2375.